Available online at www.sciencedirect.com
SCIENCE DIRECT
Journal of Colloid and Interface Science 282 (2005) 403–407
JOURNAL OF Colloid and Interface Science
www.elsevier.com/locate/jcis

The effect of surface properties on visible luminescence of nanosized colloidal ZnO membranes

Z.Y. Xiao [a], Y.C. Liu [b,*], L. Dong [a], C.L. Shao [b], J.Y. Zhang [a], Y.M. Lu [a], D.Z. Zhen [a], X.W. Fan [a]

[a] *Key Laboratory of Excited State Processes, Changchun Institute of Optics, Fine Mechanics, and Physics, Chinese Academy of Science, Changchun 130033, China*

[b] *Center for Advanced Optoelectronic Functional Material Research, Northeast Normal University, Changchun 130024, China*

Received 16 June 2004; accepted 13 August 2004

Available online 11 November 2004

Abstract

Luminescence properties of nanosized zinc oxide (ZnO) colloids depend greatly on their surface properties, which are in turn largely determined by the method of preparation. ZnO nanoparticles in the size range from 3 to 9 nm were prepared by addition of tetramethylammonium hydroxide ($(CH_3)_4NOH$) to an ethanolic zinc acetate solution. X-ray diffraction (XRD) indicates nanocrystalline ZnO membranes with polycrystalline hexagonal wurtzite structure. The ZnO membranes have a strong visible-emission intensity and the intensity depends upon hydrolysis time. The infrared spectra imply a variety of forms of zinc acetate complexes present on the surface of ZnO particles. The effect of the ZnO membrane surface properties on photoluminescence is discussed.

Keywords: Photoluminescence; Zinc acetate complexes; Sol–gel; Hydrolysis time

1. Introduction

For the past 10 year, research on quantum-size semiconductor particles has accelerated significantly due to their exciting novel optical and electrical properties [1,2]. ZnO, an important semiconductor material, has attracted considerable attention for use in short-wavelength optoelectronic devices because of its wide band gap of 3.34 eV and large exciton binding energy of 60 meV. Moreover, it is a suitable material for applications such as piezoelectric transducers, varistors, gas sensors, phosphors, and surface-acoustic-wave (SAW) devices [3–7].

To study ZnO properties and obtain high-quality thin films, a variety of techniques have been used, including molecular beam epitaxy (MBE) [8], magnetron sputtering [9], metal–organic chemical vapor deposition (MOCVD) [10], and sol–gel methods [1,11–13], to prepare ZnO thin films. In recent years, the sol–gel method has been extensively used to prepare various kinds of oxide films, such as TiO_2, $LiNbO_3$, and ITO films. In comparison to other methods, sol–gel techniques are more convenient and less expensive and have general advantages such as easier composition control and superior uniformity of product. Since the novel process of synthesizing stable ZnO colloids was reported by Spanhel ans Anderson [14], many groups have begun to pursue related research. In Ref. [14], quantized aggregation, gelation, and crystal growth in concentrated ZnO colloids were discussed in detail. Meulenkamp [15] explored the influence of temperature and water during the aging of ZnO sol. Anderson and co-workers [16] studied the luminescence properties of ZnO membranes during firing. But, to our best knowledge, no systematic investigation of the effect of variable hydrolysis time on product preparation has yet been reported in the literature.

This paper describes experiments studying the effect of hydrolysis time on the luminescence properties of thin ZnO membranes prepared by the sol–gel technique. Changes in

* Corresponding author.
E-mail address: ycliu@nenu.edu.cn (Y.C. Liu).

0021-9797/$ – see front matter
doi:10.1016/j.jcis.2004.08.111

visible luminescence at different hydrolysis times are researched in terms of changes in the surface chemistry of ZnO crystals.

2. Experimental

The preparation of colloidal suspensions was based on the method proposed by Spanhel, described briefly in Ref. [14]. The procedure consists of two major steps: (1) preparation of the precursor and (2) hydrolysis of the precursor to form the colloidal particles. A few modifications were made here. Tetramethylammonium hydroxide replaced lithium hydroxide ($LiOH{\cdot}H_2O$) as the hydrolytic agent because it is liquid at room temperature, while solid $LiOH{\cdot}H_2O$ is not easy to dissolve into ethanol. Moreover, it is difficult to remove the zinc–lithium-acetate complexes derived from $LiOH{\cdot}H_2O$ [15], whereas it is easier to remove the unwanted ionic species derived from $(CH_3)_4NOH$.

The experimental procedure was of paramount importance in controlling the chemical nature of particles obtained by hydrolysis; details are given as follows. To prepare the zinc precursor, a 0.05 M ethanolic zinc acetate $[Zn(CH_3COO)_2{\cdot}2H_2O]$ solution was magnetically stirred for 30 min at 50 °C. The flask was fitted with a condenser and a $CaCl_2$ trap to avoid moisture exposure. Tetramethylammonium hydroxide $[(CH_3)_4NOH]$ was used to hydrolyze the precursor, with hydrolysis time systematically varying between 10 and 300 min. To prevent particle growth and to remove the undesired ionic species, 0 °C hexane was used to "wash" the ZnO sol. The washed ZnO solutions were spin-coated onto *n*-type silicon and quartz substrates to form ZnO membranes, which were then heated to 100 °C for 10 min to remove residual organic solvent. The procedure of spin-coating could be repeated several times to obtain a desired film thickness.

X-ray diffraction was performed using a D/max-rA X-ray diffractometer (Rigaku) using the Cu K_α line of 1.54 Å to determine the crystal structure. Optical absorption spectra were investigated with a UV-360 spectrophotometer (Shimadzu). Infrared spectroscopic studies were conducted using a BIO-RAD FTS-3000 infrared spectrometer. Photoluminescence (PL) spectra were measured using a JY 63 Microlaser Raman spectrometer in a back-scattering geometry configuration, with a 325-nm He–Cd laser as the excitation source.

3. Results and discussion

3.1. Structural properties for ZnO membranes

Fig. 1 shows X-ray diffraction (XRD) fingerprints of two ZnO membrane samples isolated from 10-min and 90-min hydrolysis-time colloids. The diffraction peaks of the 10-min sample are broader than those of the 90-min sample, with the (002) reflection not apparent. After hydrolysis for

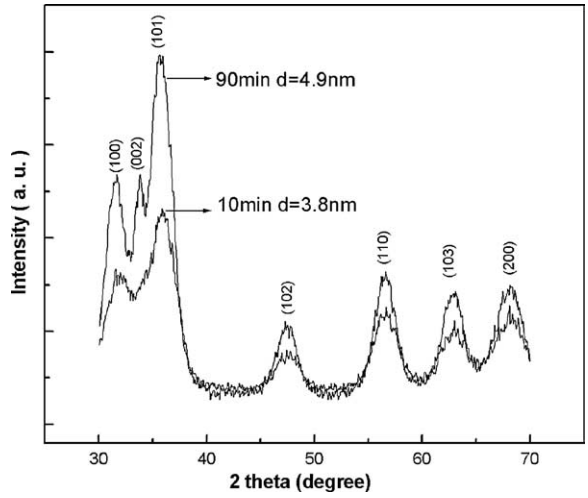

Fig. 1. The XRD patterns of the ZnO thin films at different hydrolysis times.

90 min, the diffraction peaks are more intense and narrower, while the (002) reflection becomes a peak, indicating increased crystallinity. The lattice constants calculated from the XRD pattern are $a = 3.252$ Å, $c = 5.208$ Å for the sample of 90 min and are very close to those of wurtzite ZnO, $a = 3.250$ Å, $c = 5.207$ Å [17]. This result indicates that ZnO has a polycrystalline hexagonal wurtzite structure. Average grain size was calculated using Scherrer's equation [18],

$$d = \frac{0.9\lambda}{B\cos\theta_B},$$

where λ, θ_B and B are the X-ray wavelength (1.5418 Å), Bragg diffraction angle, and linewidth at half maximum. The calculated average crystallite sizes are 3.8 and 4.9 nm in 10- and 90-min membranes, respectively.

3.2. Absorption spectra

It is known that intensities I_t and I_0 of transmitted and incident light are related by Beer's law, $I_t = I_0\exp(-\alpha L)$, where α is an absorption coefficient and L is optical path length. ZnO is a direct-band semiconductor for which α is related to the excitation energy ($E_{exc} = h\nu$) by $\alpha\ (h\nu) = A(h\nu - E_g)^{1/2}$ (for $h\nu > E_g$), where E_g is a band gap energy. Therefore, to obtain the absorption onset $\ln^2(I_t/I_0)$ is plotted versus energy, $h\nu$. Extrapolation of the linear part until it intersects the $h\nu$-axis gives E_g. Such plots for the ZnO sols prepared at various hydrolysis times are presented in Fig. 2, where the onset of absorption shifts from 3.53 to 3.38 eV as the hydrolysis time was increased from 10 min to 300 min. Such a shift in the onset of absorption indicates a decreasing optical band gap of the semiconductor, which is attributed to size quantization effects. The dependence of particle size on absorption onset can be confirmed based on an effective mass approximation,

$$E_g = E_{g0} + \frac{\hbar^2\pi^2}{2d^2}\left(\frac{1}{m_e} + \frac{1}{m_h}\right) - \frac{1.8e^2}{\varepsilon d},$$

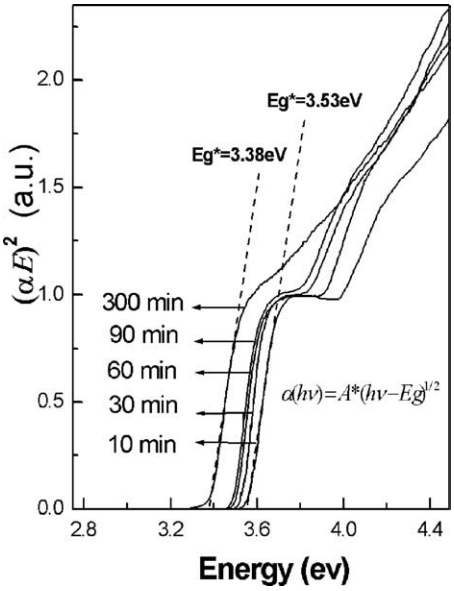

Fig. 2. Shift of the onset of absorption spectra of the ZnO sols at different hydrolysis times.

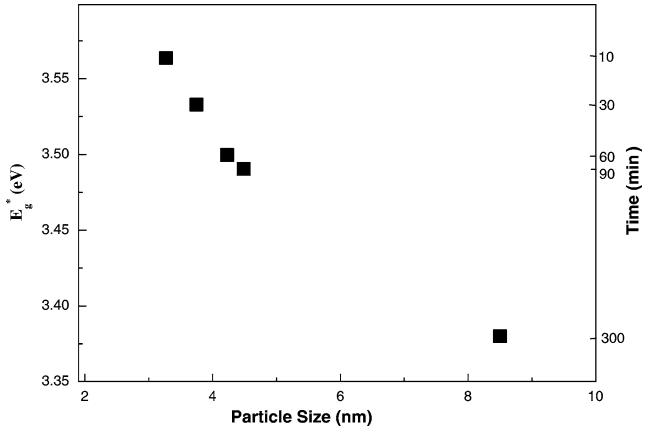

Fig. 3. The average particle size determined by the effective mass model at different hydrolysis times.

where the cluster and bulk-state band gap energies are E_g and E_{g0}, and m_e and m_h are the effective masses of an electron and a hole, respectively. Here ε is the dielectric constant of a semiconductor and d is the average particle size. Generally, it is accepted that in ZnO $E_{g0} = 3.34$ eV, $m_e = 0.24m_0$, $m_h = 0.45m_0$, $\varepsilon = 3.7$ [19]. The effect of hydrolysis time on calculated band gap energy and average particle size is shown in Fig. 3. It can be concluded that enhancing the average particle size with increasing hydrolysis time reduces the quantum confinement effect; hence a red shift in the band gap energy is observed in Fig. 3.

3.3. Photoluminescence of the ZnO membranes

Fig. 4 shows room-temperature PL spectra of ZnO films for the various hydrolysis times between 10 and 300 min. For convenience, the intensity of the near-band-edge (NBE) emission is normalized. All the spectra show near-band-edge emission and visible (vis) emission. The NBE emission peak position shifts to low energy as hydrolysis time increases. This is because the colloidal nanoparticles grow slowly and the quantum confinement effect is weakened. This is consistent with the UV/vis results above. It is remarkable that the visible emission band near 2.45 eV is observable. The inset of Fig. 4 shows the PL intensity ratios of the vis emission to the NBE emission as a function of hydrolysis time. As hydrolysis time increases from 10 to 90 min, the PL intensity ratio decreases remarkably, while it increases after 90 min. Since the colloidal ZnO particles prepared by these methods are not likely pure crystals, organic molecules (derived from precursors used in the synthesis of the colloid) adsorbed onto the surface of ZnO crystallites might affect the visible luminescence. To explain the effect of surface states on the photoluminescence, FTIR spectra were measured. The reason for the change of luminescence is revealed by analysis results of infrared (IR) spectra.

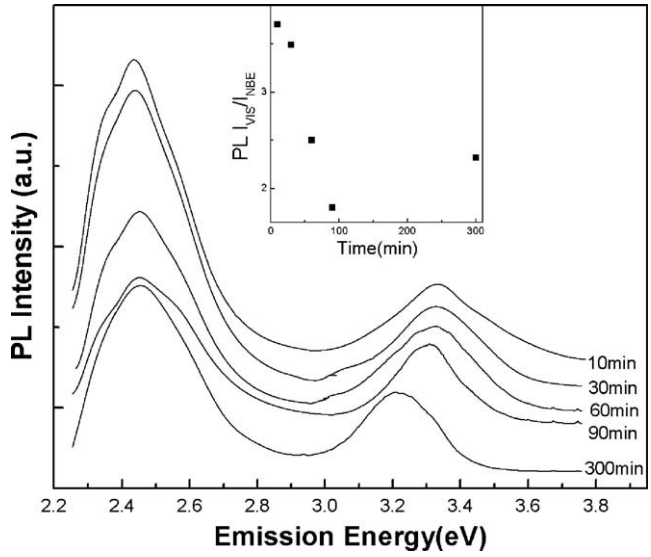

Fig. 4. Room-temperature photoluminescence spectra of the ZnO thin films at different hydrolysis time. The inset shows the ratio of intensity in the visible-emission and the near-band emission at different reaction times.

3.4. IR spectra for the ZnO membranes

Fig. 5 shows infrared (IR) spectra of samples identical to those used for PL analysis. Each spectrum has some absorption bands, and some peaks in such bands, which are nearly coincident with those typically observed for acetate groups complexed with a metal such as zinc and which correspond to C–O and C=O stretching. In general, three bonding structure are well known for acetate groups complexed with zinc. These are the unidentate, bidentate, and bridging types, as shown in Fig. 6, and the vibration frequencies in wavenumbers are listed in Table 1 [20]. It has been reported that the unidentate complex appears to be more capable of trapping a hole because it has an electron-rich free carbonyl group

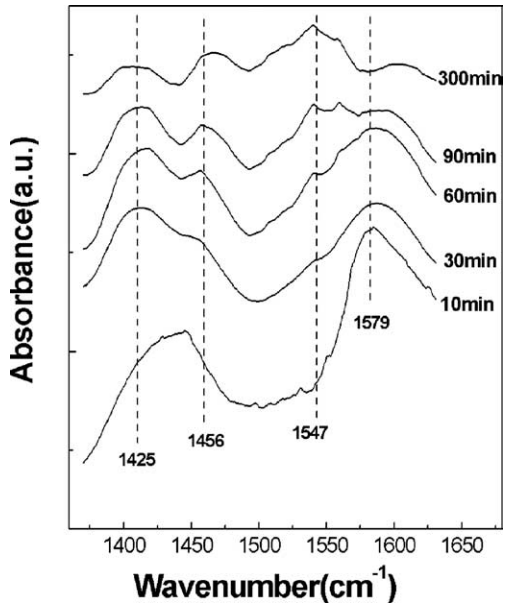

Fig. 5. Changes in the infrared spectra of ZnO films at different hydrolysis times.

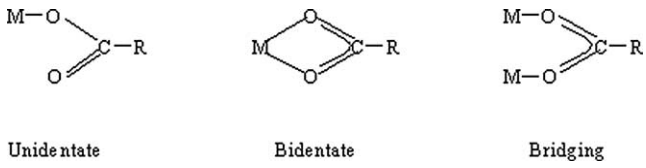

Fig. 6. Types of bonding structures for acetate and metal.

Table 1
Peak wavenumbers for various modes of acetate group coordination with metal

	$\nu_{C=O}$ (cm^{-1})	ν_{C-O} (cm^{-1})
Unidentate	1579	1425
Bidentate	1547	1456
Bridging	1600	1441

(C=O), and the bidentate form might be capable of capturing an electron [21].

As is seen in Fig. 5, various structures of acetate complexes on the surface of ZnO particles are all observed. Moreover, the vibration intensity of each mode, which indicates the amount of these complexes to some extent, depends on the hydrolysis time. Although it is difficult to give exact amounts of unidentate, bidentate, and bridging type complexes, trends can be identified by comparison of the changes in relative intensity of the absorbance bands between hydrolysis times.

The intensity of the peaks at 1547 and 1456 cm^{-1} increases, indicating a relative increase in the number of bidentate complexes with increasing hydrolysis time, while the relative number of unidentate complexes decreases. This is because bidentate complexes are thermodynamically more stable than unidentate complexes [16]. Therefore, as hydrolysis time increases, chemical reactivity decreases. For hydrolysis time 90 min, the C–O and C=O stretching intensities of unidentate and bidentate complexes appear equivalent, which implies that the numbers of unidentate and bidentate complexes are similar. As illustrated above, the unidentate and bidentate types of complexes easily trap holes and electrons, respectively. The captured hole and electron recombine through a nonradiative recombination mechanism [22]. Therefore, the intensity of visible emission has a minimum at the time of 90 min, as seen by the minimum ratio in the inset of Fig. 4. In the range of 90 min, the number of unidentate complexes, compared with that of bidentate modes, decreases gradually with increasing hydrolysis time; i.e., the density of surface-defect-bound ZnO decreases. Therefore, visible luminescence is reduced.

For hydrolysis times greater than 90 min, the intensities of peaks at 1547 and 1456 cm^{-1} continue to increase, and the number of bidentate complexes on the surfaces of ZnO particles increases. Intrinsic defects such as interstitial zinc ions (Zn_i) or oxygen vacancies (V_O) exist in ZnO particles, and at room temperature almost all V_O centers are thermally dissociated into V_O^* centers and conduction-band electrons. The V_O^* centers have an energy (2 eV) below the conduction-band edge [22]. The bidentate type of complexes easily trap photogenerated electrons, which can tunnel back into ZnO particles, where they recombine with V_O^* centers, resulting in the complexes [V_O^*, electron] or [V_O^{**}, two electrons], the recombination centers for the visible emission [23]. That is, the increase of the bidentate complexes corresponds to the increase of the concentration of the recombination centers involved in the visible luminescence of ZnO. Consequently, the visible luminescence increases after 90 min.

4. Conclusions

ZnO nanocomposite membranes were prepared in a sol–gel process using tetramethylammonium hydroxide as the hydrolyst. The ZnO colloidal particles grow gradually and the onset of the absorbance band shifts toward the red as hydrolysis time increases. The membranes show strong visible emission. Analysis of IR spectra indicated a variety of forms of acetate complexes present on the surface of ZnO particles, which absorb UV emission and affect the surface defect concentration of ZnO membranes, accounting for the observed dependence of visible emission on hydrolysis time.

Acknowledgments

This work was supported by the Program of CAS Hundred Talents, the National Fundamental Applied Research Project, the Key Project of the National Natural Science Foundation of China No. 69896260, the National Natural Science Foundation of China No. 60376009 and 60278031.

References

[1] M.S. Tokumoto, S.H. Pulcinelli, C.V. Santilli, V. Briois, J. Phys. Chem. B 107 (2003) 568.
[2] M.L. Cohen, Annu. Rev. Mater. Sci. 30 (2000) 1.
[3] D.M. Bagnall, Y.F. Chen, Z. Zhu, T. Yao, S. Koyama, M.Y. Shen, T. Goto, Appl. Phys. Lett. 70 (1997) 2230.
[4] M.T. Bjork, B.J. Ohlsson, T. Sass, A.I. Persson, C. Thelander, M.H. Magnusson, K. Deppert, L.R. Wallenberg, L. Samuelson, Appl. Phys. Lett. 80 (2002) 1058.
[5] M.H. Huang, S. Mao, H. Feick, H. Yan, Y. Wu, H. Kind, E. Weber, R. Russo, P. Yang, Science 292 (2001) 1897.
[6] Y.S. Lee, T.Y. Tseng, J. Mater. Sci. Mater. Electron. 9 (1998) 65.
[7] R. Könenkamp, K. Boedecker, M.C. Lux-Steiner, M. Poschenrieder, F. Zenia, C. Levy-Clement, S. Wagner, Appl. Phys. Lett. 77 (2000) 2575.
[8] D.M. Bagnall, Y.F. Chen, M.Y. Shen, Z. Zhu, T. Goto, T. Yao, J. Cryst. Growth 184/185 (1998) 605.
[9] N.H. Kim, H.W. Kim, Mater. Lett. 58 (2004) 938.
[10] X.T. Zhang, Y.C. Liu, L.G. Zhang, J.Y. Zhang, Y.M. Lu, D.Z. Shen, W. Xu, G.Z. Zhong, X.W. Fan, X.G. Kong, J. Appl. Phys. 92 (2002) 3293.
[11] Y. Takahashi, Y. Matsuoka, J. Mater. Sci. 23 (1988) 2259.
[12] S. Hirano, K. Kato, J. Non-Cryst. Solids 100 (1988) 538.
[13] N.J. Arfsten, J. Non-Cryst. Solids 63 (1984) 243.
[14] L. Spanhel, M.A. Anderson, J. Am. Chem. Soc. 113 (1991) 2826.
[15] E.A. Meulenkamp, J. Phys. Chem. 96 (1998) 5566.
[16] S. Sakohara, L.D. Tickanen, M.A. Anderson, J. Phys. Chem. 96 (1992) 11806.
[17] Y. Chen, D.M. Bagnall, H.K. Koh, K.T. Park, K. Hiraga, Z.Q. Zhu, T. Yao, J. Appl. Phys. 84 (1998) 3912.
[18] B.D. Cullity, Elements of X-Ray Diffractions, Addison–Wesley, Reading, MA, 1978, p. 102.
[19] L.E. Brus, J. Chem. Phys. 80 (1984) 4403.
[20] S. Sakohara, M. Ishida, M.A. Anderson, J. Phys. Chem. 102 (1998) 10,169.
[21] K. Nakamoto, Infrared and Raman Spectroscopy of Inorganic and Coordination Compounds, Wiley, New York, 1986.
[22] A.V. Dijken, E.A. Meulenkamp, D. Vanmaekelbergh, A. Meijerink, J. Phys. Chem. B 104 (2000) 1715.
[23] Y.C. Liu, X.T. Zhang, Y.M. Lu, X.G. Kong, D.Z. Shen, X.W. Fan, Chin. J. Luminesc. 23 (2002) 563.